

# Synthesis and characterization of Ni–Al<sub>2</sub>O<sub>3</sub> composite coatings containing different forms of alumina

S. T. Aruna · V. K. William Grips ·

K. S. Rajam

Received: 15 January 2010/Accepted: 5 September 2010/Published online: 17 September 2010  
© Springer Science+Business Media B.V. 2010

**Abstract** Electrodeposited Ni–Al<sub>2</sub>O<sub>3</sub> composite coatings were prepared using alumina powders synthesized from solution combustion method, precipitation method and a commercial source. Solution combustion synthesized alumina powder yielded  $\alpha$ -phase; precipitation method yielded purely  $\gamma$ -phase; commercial alumina powder was a mixture of  $\alpha$ -,  $\delta$ - and  $\gamma$ -phases. A nickel sulfamate bath was used for electro-codeposition. The current densities (0.23 A dm<sup>-2</sup> for 20 h, 0.77 A dm<sup>-2</sup> for 6 h, 1.55 A dm<sup>-2</sup> for 3 h and 3.1 A dm<sup>-2</sup> for 1.5 h) and bath agitation speeds (100, 200, 600 and 1000 rpm) were varied. The pH variations of the bath were higher during the electrodeposition of combustion synthesized alumina. The effect of different forms of alumina particles on the microhardness and microstructure of the nickel composite coating was studied. Composite coating containing combustion synthesized alumina particles was found to have higher microhardness (550 HK). It was found that at lower agitation speed (100 rpm), bigger particles were incorporated and at higher agitation speed (1000 rpm), smaller particles were incorporated. The area fraction of alumina particles incorporated in nickel matrix was highest for commercial alumina (24%). This study shows that it is not suffice to take just the current density and stirring speeds into account to explain the properties of the coatings but also to take into account the source of particles and their properties.

**Keywords** Ni · Electrodeposition · Microhardness · XRD · Alumina

## 1 Introduction

The need for coatings with improved resistance to highly aggressive environments is high due to the growing demand for extended safe service life of industrial components. Composite coatings, produced by codeposition of powders such as carbide, oxide or polymers with a metal like Ni, offer interesting engineering possibilities for purposes of wear-resistant, anti-friction and anti-seizing applications in cold-starting, dry lubrication and dispersion hardening applications [1]. Alumina (Al<sub>2</sub>O<sub>3</sub>) is one of the important dispersing ceramic particles which has been widely studied after SiC and Si<sub>3</sub>N<sub>4</sub>. Al<sub>2</sub>O<sub>3</sub> is the most cost effective and widely used material in the family of engineering ceramics. Al<sub>2</sub>O<sub>3</sub> has mechanical and physical properties particularly suitable for electrical and thermal insulation, for cutting tools and abrasives. It also has very good anti-corrosion properties. Al<sub>2</sub>O<sub>3</sub> is known to undergo a series of crystal structural transformations starting from  $\gamma$ -Al<sub>2</sub>O<sub>3</sub> to the most stable form  $\alpha$ -Al<sub>2</sub>O<sub>3</sub> as follows:  $\gamma \rightarrow \delta \rightarrow \theta \rightarrow \alpha$ .  $\alpha$ -Al<sub>2</sub>O<sub>3</sub> is the strongest and stiffest of the oxide ceramics. Its high hardness, excellent dielectric properties, refractoriness and good thermal properties make it the material of choice for a wide range of applications. The two common crystal structures of alumina are the harder  $\alpha$ -Al<sub>2</sub>O<sub>3</sub> (Mohs hardness 9) and the softer-Al<sub>2</sub>O<sub>3</sub> crystal structure (Mohs hardness 8).<sup>1</sup>  $\alpha$ -Al<sub>2</sub>O<sub>3</sub> is composed of trigonal crystals with sp. gr. about 3.987 and  $\gamma$ -Al<sub>2</sub>O<sub>3</sub> is composed of minute colorless cubic crystals with sp. gr. about 3.67 that are transformed to the alpha form at high temperatures.

S. T. Aruna (✉) · V. K. William Grips · K. S. Rajam  
Surface Engineering Division, Council of Scientific  
and Industrial Research-National Aerospace Laboratories,  
Post Bag No. 1779, Bangalore 560 017, India  
e-mail: aruna\_reddy@nal.res.in

<sup>1</sup> <http://www.metallographic.com/Industrial%20Products/Alumina.htm>.

Improved properties for Ni–Al<sub>2</sub>O<sub>3</sub> composites containing  $\alpha$ -Al<sub>2</sub>O<sub>3</sub> prepared using sedimentation technique from Watt's type bath has been reported [2]. Dong et al. prepared graded Ni–Al<sub>2</sub>O<sub>3</sub> coating using a polyhedron rotating cathode [3]. Single layer and discretely stepped electrocomposites consisting of a metallic nickel matrix with second phase alumina particles (phase not mentioned) were prepared from a sulfamate bath by Banovic et al. [4]. Al<sub>2</sub>O<sub>3</sub>, TiO<sub>2</sub>, Si<sub>3</sub>N<sub>4</sub>, diamond nano-particle strengthened nickel-based brush plating composite coatings were prepared by co-deposition of nano-particles with Ni metal-matrix [5]. The influence of the presence of particles on crystallization behaviour, residual stress and texture of the deposited nickel coatings containing Al<sub>2</sub>O<sub>3</sub> and TiO<sub>2</sub> has also been reported [6]. Bund and Thiemig have studied the influence of bath composition and pH on the electrodeposition of Al<sub>2</sub>O<sub>3</sub> nanoparticles and nickel [7]. Effect of some operating variables on the characteristics of electrodeposited Ni– $\alpha$ -Al<sub>2</sub>O<sub>3</sub> and Ni–TiO<sub>2</sub> composites have been reported by Fawzy et al. [8]. Shao et al. have described a kinetic model for electrochemical deposition of metal matrix nanocomposites containing inert particles like Al<sub>2</sub>O<sub>3</sub> taking into account both the diffusion force as well as the gravitational force acting on the particles [9]. They have shown that for codeposition of 300 nm Al<sub>2</sub>O<sub>3</sub> particles in Ni, gravitational force has to be taken into account and for 50 nm particles it is negligible. Improved yield strength has been reported for electrodeposited Ni–Al<sub>2</sub>O<sub>3</sub> from a Watt's type nickel electrolyte [10]. The corrosion resistance of composite nickel electrodeposits with Al<sub>2</sub>O<sub>3</sub> embedded in the nickel matrix prepared in sulfate and chloride bath has been studied. [11]. Improved corrosion resistance of Ni–Al<sub>2</sub>O<sub>3</sub> ( $\alpha$ -phase) electrochemically deposited from a Watts bath has been reported [12]. Thiemig et al. have also reported improved microhardness for nickel alumina nanocomposites prepared using an impinging jet electrode [13]. Chen et al. studied the effect of pulse frequency on the microstructure, hardness and wear resistance of Ni–Al<sub>2</sub>O<sub>3</sub> composite coatings [14]. Wei et al. have determined the Young's modulus of electrochemically co-deposited Ni–Al<sub>2</sub>O<sub>3</sub> nanocomposite and showed that it can be considerably increased by incorporation of fumed  $\alpha$ -Al<sub>2</sub>O<sub>3</sub> nanoparticles into the Ni matrix. [15]. Electrochemical impedance spectroscopy and corrosion behaviour of Ni–Al<sub>2</sub>O<sub>3</sub> nanocomposite coatings has been reported by Benea et al. [16]. The authors have used Al<sub>2</sub>O<sub>3</sub> nanoparticles (13 nm), however the phase and source of alumina powder is not reported.

During the past 40 years Cu–Al<sub>2</sub>O<sub>3</sub> codeposition systems have been extensively studied. There have been contradictory reports about the codeposition of  $\gamma$ -Al<sub>2</sub>O<sub>3</sub>. Hoffmann [17] and Sauter [18] confirmed the impossibility of  $\gamma$ -Al<sub>2</sub>O<sub>3</sub> deposition from copper sulphate baths. Chen

et al. reported the feasibility of codeposition of  $\alpha$ -Al<sub>2</sub>O<sub>3</sub> and the impossibility of  $\gamma$ -Al<sub>2</sub>O<sub>3</sub> incorporation with copper from sulphate baths [19]. Most of the literature available discusses the synthesis and properties of Ni-composite coating containing mostly  $\alpha$ -Al<sub>2</sub>O<sub>3</sub>. To the best of our knowledge there are no reports on the comparative study on the properties of Ni-composite coating containing different forms of alumina prepared by different methods. It is interesting to investigate the effect of different forms of alumina on the properties of the Ni-alumina composite coatings. The aim of this work was (i) to prepare Al<sub>2</sub>O<sub>3</sub> powders by different methods; (ii) to prepare Ni–Al<sub>2</sub>O<sub>3</sub> composite coatings containing alumina particles synthesized from different methods, (iii) compare the microhardness of Ni-Al<sub>2</sub>O<sub>3</sub> composites and (iv) to study the effect of stirring speed on the properties of the composite coatings. From the literature it appears that agitation speed and current density are important parameters during codeposition [1]. Therefore, in this study the effect of stirring speed on the particle incorporation and in turn on the microhardness of Ni–Al<sub>2</sub>O<sub>3</sub> composite coatings has been studied.

## 2 Experimental

### 2.1 Preparation of alumina particles and characterization of powders

Pure  $\alpha$ -Al<sub>2</sub>O<sub>3</sub> was prepared using aluminium nitrate as oxidizer and ammonium acetate and urea as fuel. Solution combustion method has been used for the preparation of all types of oxides because of the simplicity, and ease of this process [20].  $\alpha$ -Al<sub>2</sub>O<sub>3</sub> (alumina-1) was synthesized from solution combustion method by using analytical grade chemicals like Al(NO<sub>3</sub>)<sub>3</sub>·9H<sub>2</sub>O (225 g), urea (68 g) and ammonium acetate (16 g). During combustion, a low intensity flame existed for a very short duration and resulted in a foamy white mass which was identified as  $\alpha$ -Al<sub>2</sub>O<sub>3</sub>. Gamma-alumina (alumina-2) was prepared by precipitation method using analytical grade aluminium nitrate as the precursor and ammonium carbonate as precipitating agent. In a typical experiment, 100 g aluminum nitrate was dissolved in distilled water to which 4.8 M ammonium carbonate solution was added drop wise until the pH of the solution raised to 10. The precipitation was carried out at room temperature. The precipitate was allowed to settle, followed by filtration and drying at 120 °C for 12 h. The dried powder was calcined at 900 °C for 8 h.

The powders were characterized for phase identification and crystallite size determination using a Powder X-Ray diffractometer (Rigaku D/max 2200) with CuK<sub>α</sub> radiation. The morphology of the powders was determined by Leo

440I Scanning Electron Microscope. The Raman spectra of the powders were recorded with a DILOR-JOBIN-YVON-SPEX (Paris, France) integrated Raman Spectrometer (Model Labram). The particle size distribution of the powders was determined using Mastersizer 2000 (Malvern instruments) and the zeta potential of the powders in nickel sulphamate bath solution was determined using Malvern zeta sizer. A magnetic stirrer with variable rpm (Remi, India) was used for keeping the particles in suspension.

## 2.2 Preparation and characterization of Ni-alumina composite coatings

Nickel sulfamate plating bath was prepared by mixing 300 g L<sup>-1</sup> of nickel sulfamate solution (50 g of nickel per litre), 10 g L<sup>-1</sup> of nickel chloride, 30 g L<sup>-1</sup> boric acid and 0.2 g L<sup>-1</sup> of sodium lauryl sulfate. The Ni-sulfamate plating bath (~200 mL) containing 20 g Al<sub>2</sub>O<sub>3</sub> particles (100 g/L) in a glass beaker was held at room temperature and its pH was maintained at 4 by the addition of sulfamic acid and basic nickel carbonate. A pure nickel sheet (2.5 cm × 12 cm) and a brass substrate of the same dimension were used as anode and cathode respectively. The polished brass substrate of area 2.5 cm × 3.75 cm was degreased with acetone followed by cathodic cleaning and acid dipping and finally washed with distilled water. In order to ensure uniform dispersion of the powder, the electrolyte bath containing particles was subjected to magnetic stirring (~600 rpm) for 15 h before the deposition process and during electrodeposition the particles were also magnetically stirred at various rpm (100, 200, 600 and 1000). The codeposition was carried out at various current densities: 0.23 A dm<sup>-2</sup> for 20 h, 0.77 A dm<sup>-2</sup> for 6 h, 1.55 A dm<sup>-2</sup> for 3 h and 3.1 A dm<sup>-2</sup> for 1.5 h such that the deposit thickness was ~40 µm based on Faraday's laws. The following notations were used for indicating the Ni composite coatings as: (i) Ni-Al<sub>2</sub>O<sub>3</sub>-1 (containing combustion synthesized Al<sub>2</sub>O<sub>3</sub>), (ii) Ni-Al<sub>2</sub>O<sub>3</sub>-2 (containing precipitation synthesized Al<sub>2</sub>O<sub>3</sub>) and (iii) Ni-Al<sub>2</sub>O<sub>3</sub>-3 (containing commercial Al<sub>2</sub>O<sub>3</sub> (Alcoa)).

The cross-sectional metallographic specimens were prepared by sandwiching electrodeposited Ni-Al<sub>2</sub>O<sub>3</sub> brass coupons with a copper backup in a Bakelite matrix followed by mechanical grinding and polishing with Al<sub>2</sub>O<sub>3</sub> slurry, down to 0.05 µm. The microhardness measurements were performed on ten different locations on the cross-section of each coating (Micromet 2103, Buehler, 50 gf load). The optical micrographs of the cross sections of Ni-Al<sub>2</sub>O<sub>3</sub> were recorded using a vertical metallurgical microscope. The area fraction of particles incorporated in the Ni matrix was calculated from the cross-sectional optical micrographs using image analysis software (Videopro 32 supplied by M/s Leading Edge, Australia).

FESEM images of the cross-sections of Ni-Al<sub>2</sub>O<sub>3</sub> were also recorded (Carl Zeiss).

## 3 Results and discussions

### 3.1 Characterization of alumina powders

The combustion synthesized Al<sub>2</sub>O<sub>3</sub> powder (Al<sub>2</sub>O<sub>3</sub>-1) exhibited pure  $\alpha$ -phase as shown in the powder XRD pattern (Fig. 1c). The crystallite size of Al<sub>2</sub>O<sub>3</sub>-1 as calculated from Scherrer equation was 40 nm. The powder XRD pattern of precipitated Al<sub>2</sub>O<sub>3</sub> powder (Al<sub>2</sub>O<sub>3</sub>-2) showed pure  $\gamma$ -phase and the crystallite size was 5 nm (Fig. 1a). The commercial Al<sub>2</sub>O<sub>3</sub> powder (Al<sub>2</sub>O<sub>3</sub>-3) exhibited a mixture of  $\alpha$ - and  $\gamma$ -phases as shown in the XRD pattern (Fig. 1b) and the crystallite size was 45 nm. A small peak between 10 and 15° corresponding to  $\delta$ -phase was also observed for Al<sub>2</sub>O<sub>3</sub>-3 (Fig. 1b). The Raman spectrum of

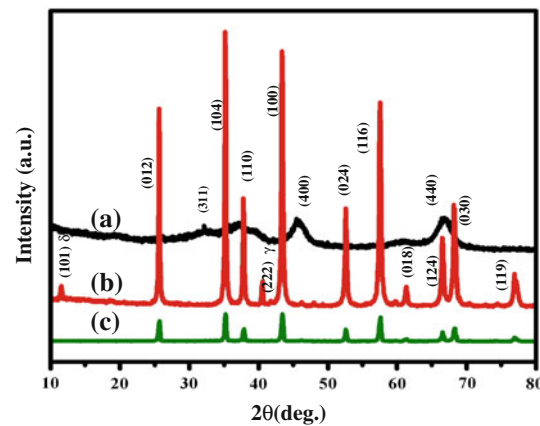


**Fig. 1** Powder XRD patterns of (a) precipitation synthesized (Al<sub>2</sub>O<sub>3</sub>-2) (b) commercial alumina (Al<sub>2</sub>O<sub>3</sub>-3) powders and (c) combustion synthesized (Al<sub>2</sub>O<sub>3</sub>-1)

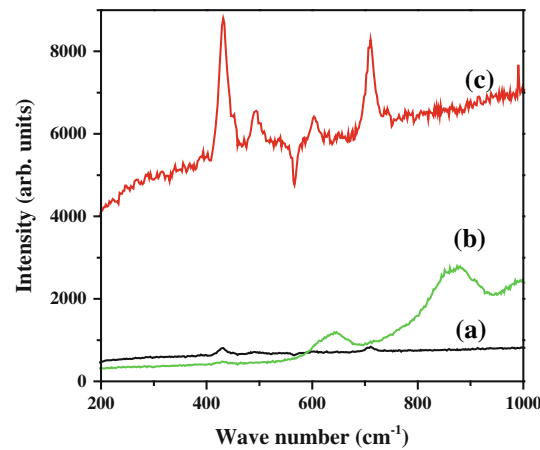


**Fig. 2** Raman spectra of (a) Al<sub>2</sub>O<sub>3</sub>-1 (b) Al<sub>2</sub>O<sub>3</sub>-2 and (c) Al<sub>2</sub>O<sub>3</sub>-3

$\text{Al}_2\text{O}_3$ -1 (Fig. 2a) shows peaks at 429, 489 and  $710 \text{ cm}^{-1}$  corresponding to high temperature  $\alpha$ - $\text{Al}_2\text{O}_3$ . The Raman spectrum of  $\text{Al}_2\text{O}_3$ -2 (Fig. 2b) shows peaks at 429, 489, 599, 710 and  $990 \text{ cm}^{-1}$ . The peaks at 429, 489 and  $710 \text{ cm}^{-1}$  are common to both samples 1 and 2 which indicates the presence of  $\alpha$ - $\text{Al}_2\text{O}_3$  in amorphous state in alumina-2 which cannot be revealed in XRD. The Raman spectrum of  $\text{Al}_2\text{O}_3$ -3 shows peaks at 418, 636, 861, 988 and  $1094 \text{ cm}^{-1}$  (Fig. 2c). As reported by Porto and Krishnan, the Raman active phonon modes for corundum ( $\alpha$ - $\text{Al}_2\text{O}_3$ ) appear at 378, 418, 432, 451, 578, 645 and  $751 \text{ cm}^{-1}$  [21]. Only one Raman band ( $429 \text{ cm}^{-1}$ ) in our spectra matches close to the reported Raman band of corundum. The other sharp bands could have come from plasma lines of laser [22].

The SEM images of the powders at lower magnification showed flaky morphology for  $\text{Al}_2\text{O}_3$ -1 and  $\text{Al}_2\text{O}_3$ -2 powders. The SEM of alumina-3 showed irregular shaped nanoparticles with agglomeration. Hence high resolution FESEM images (Fig. 3a–c) were recorded for all the powders. The FESEM image of  $\text{Al}_2\text{O}_3$ -1 (Fig. 3a) showed large number of irregular shaped agglomerates containing smaller spherical particles ( $\leq 50 \text{ nm}$ ).  $\text{Al}_2\text{O}_3$ -2 (Fig. 3b) showed agglomerates made of smaller particles ( $\leq 50 \text{ nm}$ ).  $\text{Al}_2\text{O}_3$ -3 showed spherical to irregular shaped particles with various sizes as low as  $50 \text{ nm}$  and as high as  $1 \mu\text{m}$ .

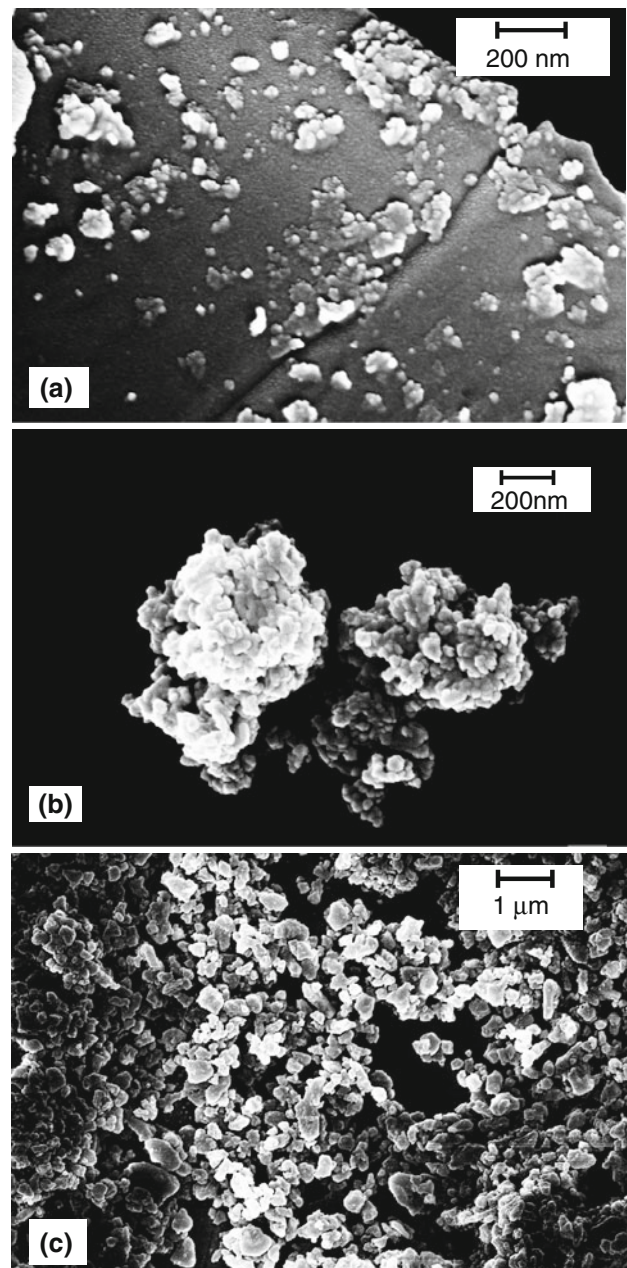
The average agglomerated particle sizes were 15, 3.6 and  $2 \mu\text{m}$  respectively for  $\text{Al}_2\text{O}_3$ -1,  $\text{Al}_2\text{O}_3$ -2 and  $\text{Al}_2\text{O}_3$ -3 as determined by particle size analyzer. This indicates higher agglomeration of combustion synthesized powder. The zeta potential for  $\text{Al}_2\text{O}_3$ -1,  $\text{Al}_2\text{O}_3$ -2 and  $\text{Al}_2\text{O}_3$ -3 was +27, +10.8 and +22 mV respectively. The positive zeta potential indicates a positive charge on the  $\text{Al}_2\text{O}_3$  particles which favours the inclusion of particles in the growing nickel film.

### 3.2 Characterization of Ni– $\text{Al}_2\text{O}_3$ coatings

It is interesting to note that unlike in Cu matrix, both  $\alpha$  and  $\gamma$ - $\text{Al}_2\text{O}_3$  particles could be easily codeposited with Ni matrix.

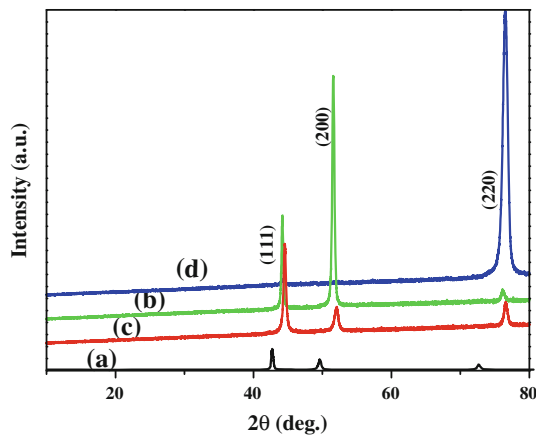
#### 3.2.1 The effect of particle incorporation on Ni crystallite size and Ni orientation

Figure 4 shows XRD patterns of Ni and Ni– $\text{Al}_2\text{O}_3$  coatings electrodeposited at  $1.55 \text{ A dm}^{-2}$  with a stirring speed of 600 rpm. Pure Ni coatings showed intense (111) diffraction line along with (200) diffraction lines and this corresponds to [111] texture. The diffraction pattern of Ni– $\text{Al}_2\text{O}_3$ -1 is characterized by an intense (200) diffraction line corresponding to a [100] texture (Fig. 4a). In case of Ni– $\text{Al}_2\text{O}_3$ -2, [111] texture similar to pure Ni was observed and diffraction lines corresponding to (200) and (220) were also



**Fig. 3** FESEM images of **a**  $\text{Al}_2\text{O}_3$ -1, **b**  $\text{Al}_2\text{O}_3$ -2 and **c**  $\text{Al}_2\text{O}_3$ -3 powders

observed (Fig. 4b). In case of Ni– $\text{Al}_2\text{O}_3$ -3, the intense diffraction peak corresponded to (220), a minor peak corresponding to (111) was observed and (200) peak was not observed (Fig. 4c). The textural developments are usually attributed to the existence or formation of different chemical species in the catholyte during the cathodic process [23]. Accordingly, the [211] texture has been attributed to the presence of a colloidal dispersion of nickel hydroxide  $[\text{Ni}(\text{OH})_2]$ ; [110] texture to the presence of atomic hydrogen or to the combined action of both molecular hydrogen and  $[\text{Ni}(\text{OH})_2]$ ; and [100] texture is



**Fig. 4** XRD patterns of (a) Ni (b) Ni-Al<sub>2</sub>O<sub>3</sub>-1, (c) Ni-Al<sub>2</sub>O<sub>3</sub>-2 and (d) Ni-Al<sub>2</sub>O<sub>3</sub>-3 composite coatings on brass substrate electrodeposited at 1.55 A/dm<sup>2</sup>

considered as free of inhibiting chemical species. According to the observed pH variations, we expect Ni-Al<sub>2</sub>O<sub>3</sub>-1 with hydroxyl groups to possess [211] texture, instead [100] texture was observed. This indicates that the preparation method and different phases of Al<sub>2</sub>O<sub>3</sub> particles embedded in the coatings can affect the preferred orientation of the Ni metal matrix.

The Ni grain sizes as calculated from Scherrer formula were 25, 16 and 11 nm respectively for Ni-Al<sub>2</sub>O<sub>3</sub>-1, Ni-Al<sub>2</sub>O<sub>3</sub>-2 and Ni-Al<sub>2</sub>O<sub>3</sub>-3.

### 3.2.2 Effect of different phases of alumina on the microstructure of Ni deposit

The surface SEM images of Ni-Al<sub>2</sub>O<sub>3</sub> coatings are shown in Fig. 5. It is evident that the surface of Ni-Al<sub>2</sub>O<sub>3</sub>-2 exhibits only nodular structure which may be influenced by the  $\gamma$  phase of alumina. This is further substantiated by the fact that Ni-Al<sub>2</sub>O<sub>3</sub>-3 which is a mixture of  $\alpha$ ,  $\gamma$  and  $\delta$  phases exhibits a mixture of nodular and smooth surfaces and the same microstructure is absent in Ni-Al<sub>2</sub>O<sub>3</sub>-1 which contains only pure  $\alpha$  phase.

### 3.2.3 The effect of magnetic stirring speed on particle incorporation and microhardness

The pH of the nickel sulfamate bath before and after electrodepositions was recorded. For Ni-Al<sub>2</sub>O<sub>3</sub>-1, the pH variations of the Ni sulfamate bath during electrodeposition was not significant ( $\sim 0.1$ ) at lower rpm's for all current densities. At the highest rpm (1000), the pH variation was very high ( $\sim 1$ ). On the other hand for Ni-Al<sub>2</sub>O<sub>3</sub>-2 and Ni-Al<sub>2</sub>O<sub>3</sub>-3 baths, the pH variations were not significant during electrodeposition. To explore the probable reason for this variation, a set of experiments were conducted by

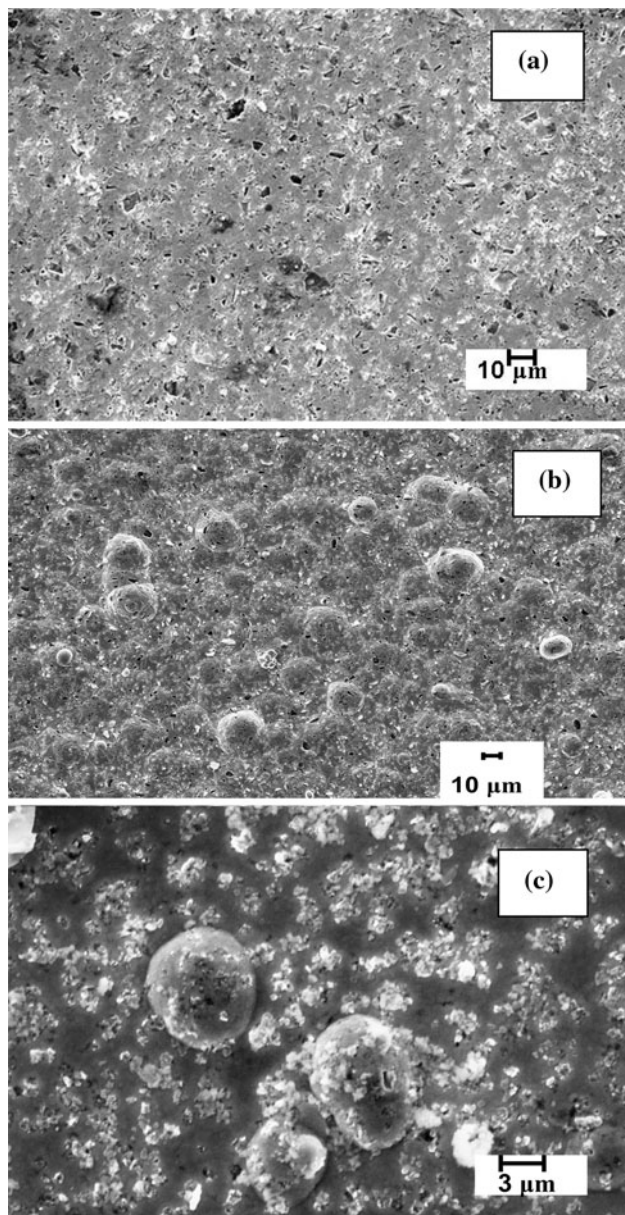


**Fig. 5** SEM images of the surfaces of **a** Ni-Al<sub>2</sub>O<sub>3</sub>-1, **b** Ni-Al<sub>2</sub>O<sub>3</sub>-2 and **c** Ni-Al<sub>2</sub>O<sub>3</sub>-3

adding 100 g of Al<sub>2</sub>O<sub>3</sub>-1, Al<sub>2</sub>O<sub>3</sub>-2 and Al<sub>2</sub>O<sub>3</sub>-3 to 1 l of distilled water. The initial pH of the water with the particles was noted down and stirred at two different rpm (200 and 1000) for 3 h and the final pH was measured. It was found that only in case of Al<sub>2</sub>O<sub>3</sub>-1 with 1000 rpm, the pH variation was higher ( $\sim 0.8$ ) and at lower rpm the variation was less ( $\sim 0.2$ ). For the other two powders, the variation was not significant. This may be probably due to the differences in the amount of hydroxyl groups present on the Al<sub>2</sub>O<sub>3</sub> powders. The higher amount of hydroxyl groups for Al<sub>2</sub>O<sub>3</sub>-1 powder may be due to the method of preparation. In case of Al<sub>2</sub>O<sub>3</sub>-1 preparation by solution combustion process, the flame exists for very short duration and the

flame temperature would have been just sufficient for the crystallization of alumina. On the other hand in case of  $\text{Al}_2\text{O}_3$ -2, the powders were calcined at 900 °C for 8 h during which the surface hydroxyl groups would have escaped.

The plots of microhardness versus the magnetic stirring speeds for  $\text{Ni}-\text{Al}_2\text{O}_3$ -1,  $\text{Ni}-\text{Al}_2\text{O}_3$ -2 and  $\text{Ni}-\text{Al}_2\text{O}_3$ -3 electrodeposited at 0.23, 1.55 and 3.1 A  $\text{dm}^{-2}$  current densities are shown in Figs. 6, 7, 8.  $\text{Ni}-\text{Al}_2\text{O}_3$ -1 showed higher microhardness values at almost all rotating speeds and current densities. Attempts were made to correlate the microhardness with the texture of the coatings electrodeposited at 1.55 A  $\text{dm}^{-2}$  at 600 rpm. According to literature, the microstructure corresponding to [100] texture is associated to deposits with maximum ductility, minimum hardness and internal stresses [23]. But in the present

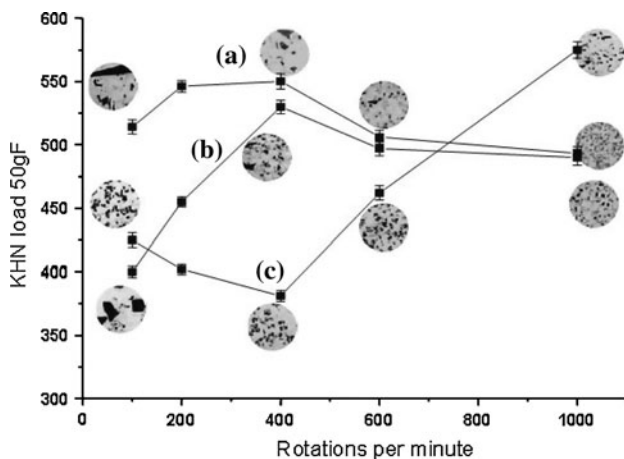


**Fig. 6** Plots of microhardness vs. the magnetic stirring speed (rpm) along with the corresponding inserts of cross-sectional optical micrographs of (a)  $\text{Ni}-\text{Al}_2\text{O}_3$ -1, (b)  $\text{Ni}-\text{Al}_2\text{O}_3$ -2 and (c)  $\text{Ni}-\text{Al}_2\text{O}_3$ -3 electrodeposited at 0.23 A/ $\text{dm}^2$

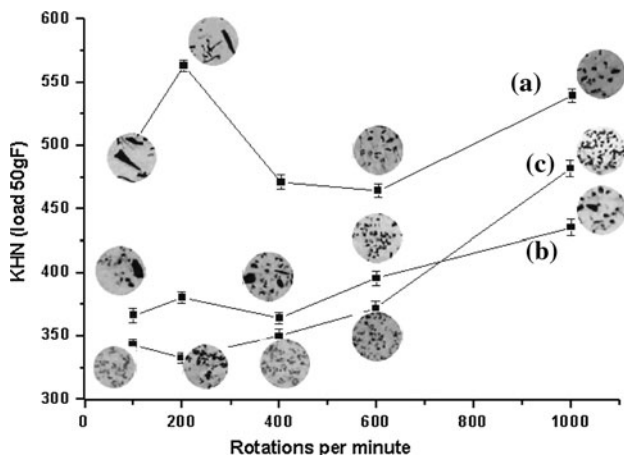


**Fig. 7** Plots of microhardness vs. the magnetic stirring speed (rpm) along with the corresponding inserts of cross-sectional optical micrographs of (a)  $\text{Ni}-\text{Al}_2\text{O}_3$ -1, (b)  $\text{Ni}-\text{Al}_2\text{O}_3$ -2 and (c)  $\text{Ni}-\text{Al}_2\text{O}_3$ -3 electrodeposited at 1.55 A/ $\text{dm}^2$

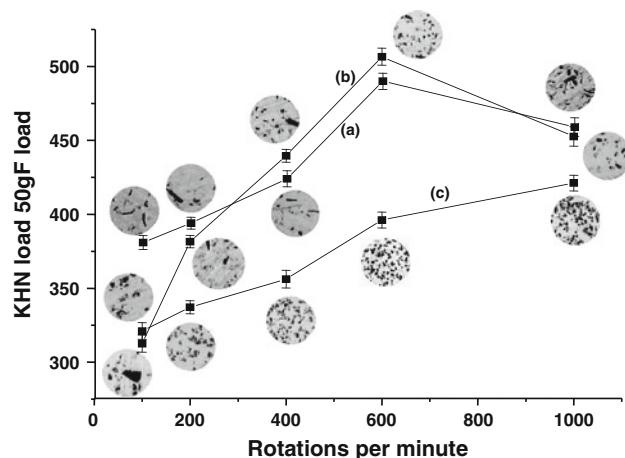


**Fig. 8** Plots of microhardness vs. the magnetic stirring speed (rpm) along with the corresponding inserts of cross-sectional optical micrographs of (a)  $\text{Ni}-\text{Al}_2\text{O}_3$ -1, (b)  $\text{Ni}-\text{Al}_2\text{O}_3$ -2 and (c)  $\text{Ni}-\text{Al}_2\text{O}_3$ -3 electrodeposited at 3.1 A/ $\text{dm}^2$

study,  $\text{Ni}-\text{Al}_2\text{O}_3$ -1 with [100] texture has yielded maximum hardness. It is known that the hardness of metal matrix composites depend on the amount and the size of the dispersed phase, apart from the mechanical characteristics of the matrix, particles and interfaces [23]. The observed higher microhardness for  $\text{Ni}-\text{Al}_2\text{O}_3$ -1 may be attributed to the larger agglomerated size of alumina particles. Cross-sectional optical micrographs of a few selected  $\text{Ni}-\text{Al}_2\text{O}_3$  composite coatings recorded at a magnification of 1000× are shown as inserts in Figs. 6, 7, 8. The following inferences can be drawn from the optical images and microhardness data:

- Irrespective of the current densities used for electrodeposition, lowest rpm results in larger agglomerated particles in case of  $\text{Ni}-\text{Al}_2\text{O}_3$ -1 and  $\text{Ni}-\text{Al}_2\text{O}_3$ -2. This phenomenon is not predominantly seen in  $\text{Ni}-\text{Al}_2\text{O}_3$ -3.
- Irrespective of the current densities always smaller particles were incorporated at highest rotation speed (1000 rpm).
- The variation of microhardness versus rotation speed showed similar trend in case of  $\text{Ni}-\text{Al}_2\text{O}_3$ -1 and  $\text{Ni}-\text{Al}_2\text{O}_3$ -2 that is minima followed by maxima and then minima. The trend was reversed in case of  $\text{Ni}-\text{Al}_2\text{O}_3$ -3.
- Higher current density resulted in lower microhardness which was due to the less number of particles incorporated. This is due to the fact that the rate of Ni deposition is higher at higher current density which results in higher rate of metal deposition and the chance entrapment of  $\text{Al}_2\text{O}_3$  particle is less.
- $\text{Ni}-\text{Al}_2\text{O}_3$ -1 always exhibited higher microhardness values. This may be due to the presence of larger agglomerated particles observed in  $\text{Ni}-\text{Al}_2\text{O}_3$ -1.

- (vi) In the case of Ni-Al<sub>2</sub>O<sub>3</sub>-1, larger agglomerates with thread like particles were observed.
- (vii) The particle distribution was found to be much more uniform and more particles were incorporated in Ni-Al<sub>2</sub>O<sub>3</sub>-3 probably due to the presence of a dispersing agent in the commercial alumina powder.

The cross-sectional FESEM images of Ni-Al<sub>2</sub>O<sub>3</sub>-1, Ni-Al<sub>2</sub>O<sub>3</sub>-2 and Ni-Al<sub>2</sub>O<sub>3</sub>-3 electrodeposited at 1.55 A dm<sup>-2</sup> (1000 rpm) are shown in Figs. 9, 10, 11. In case of Ni-Al<sub>2</sub>O<sub>3</sub>-1, irregular thread like particles with less agglomeration is observed (Fig. 9a, b). Ni-Al<sub>2</sub>O<sub>3</sub>-2 consisted of agglomerated odd shaped particles (Fig. 10a, b) and Ni-Al<sub>2</sub>O<sub>3</sub>-3 consisted of large number of particles with odd shapes (Fig. 11a and b). The area fraction of particles incorporated in the Ni matrix was the highest for Ni-Al<sub>2</sub>O<sub>3</sub>-3 (11–24%) followed by Ni-Al<sub>2</sub>O<sub>3</sub>-2 (7–15%) and Ni-Al<sub>2</sub>O<sub>3</sub>-1 (4–13%).

From this study it is evident that the source of particles, its properties (phase purity, particle shape, size, size distribution etc.), stirring speeds and current density are some of the factors which will influence the properties of the composite coating. In the literature there have been deviations observed in the experimental and theoretical curves of composite coatings derived from the Guglielmi model

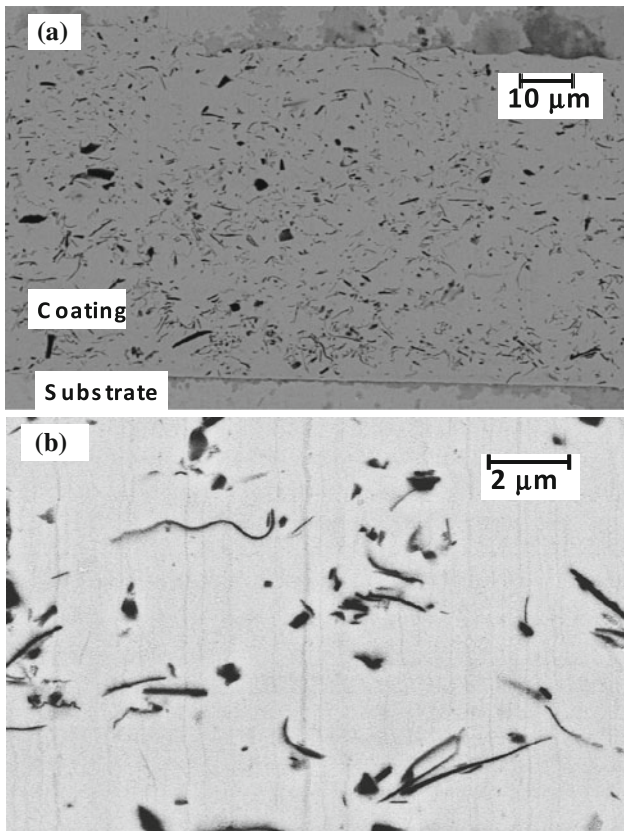


**Fig. 9** FESEM cross-sectional image of Ni-Al<sub>2</sub>O<sub>3</sub>-1 **a** 2.5 KX and **b** 15 KX

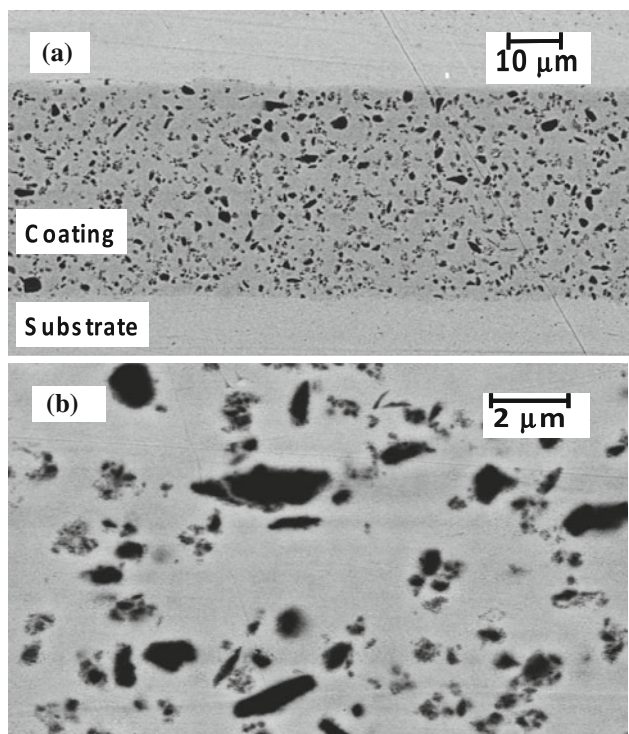


**Fig. 10** FESEM cross-sectional image of Ni-Al<sub>2</sub>O<sub>3</sub>-2 **a** 2.5 KX and **b** 15 KX

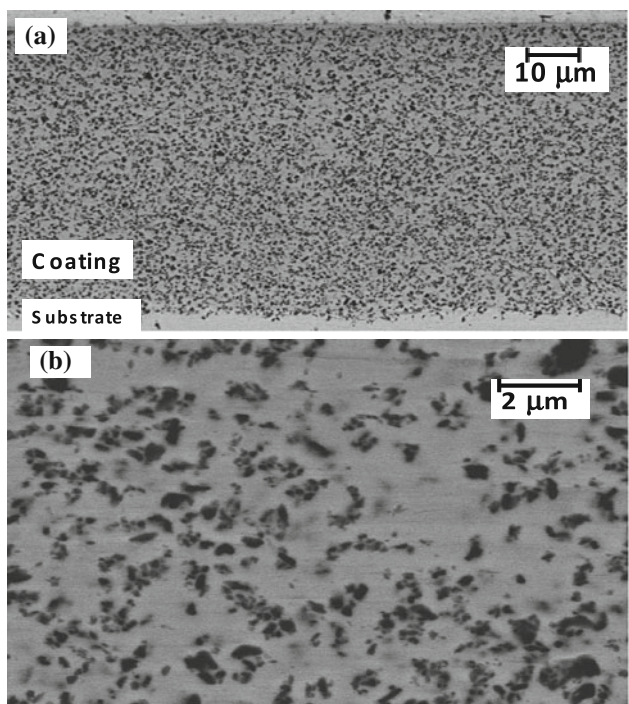


**Fig. 11** FESEM cross-sectional image of Ni-Al<sub>2</sub>O<sub>3</sub>-3 **a** 2.5 K X and **b** 15 K X

[24]. This means that there are other parameters that are to be taken into account in this model. Celis and Roos [25] and Buelens [26], in their model based on a statistical

approach, included the effects of several parameters of the process that Guglielmi neglected, such as the adsorption of ionic species on the particle surface, the particle nature, the ions to be reduced, the bath components and the hydrodynamic conditions. Their model could include solid particles and fine metal particles and their model has the advantage of being validated with particles of 0.05 μm diameter. All these models have been derived mostly using rotating disk electrodes for controlling the hydrodynamic conditions. Fransaer et al. [27] developed a particle trajectory model for micron size particles, based on all forces and torques acting on a particle like gravity, electrophoretic force and the double layer force. This model fails close to the electrode surface because it leads to the “perfect sink”. They introduced the particle-electrode interaction term, introducing a new equation for the probability that a particle at the electrode surface will be incorporated, which gives a good description of the variation of the amount of particles in the deposits as a function of the bath particle concentration. However, this trajectory model does not predict a maximum particle concentration with respect to current density, and it is not applicable to nanosize particles where Brownian motion is expected to dominate. Although many theoretical models have been proposed, the flexibility and reliability of each to describe the behavior of a wide range of metallic coatings and particle types still requires validation [28]. The effects of particle inclusion on deposit electrocrystallisation have to be considered in the models as the inclusion of particles into a metal deposit may cause (i) reduction of the cathode surface area in case of nonconductive particles and (ii) enlargement of the cathode surface area in case of conductive particles (iii) modification of the deposit morphology [28].

In the present study we have also observed that the Ni deposit morphology varied with the different forms of alumina particles incorporation. From this study we observe that in all the models available so far, the effects of (i) the particle size, particle shape and particle size distribution (ii) the phase of the particles (crystallographic orientation planes) has not been considered. Applying these models and adding corrective factors for studying the electrodeposition of Ni-Al<sub>2</sub>O<sub>3</sub> composite coatings containing Al<sub>2</sub>O<sub>3</sub> particles of different phases and different particle size distribution is beyond the scope of the present work and will be taken up in future. The effect of different phases of Al<sub>2</sub>O<sub>3</sub> on the corrosion and wear resistance of Ni-Al<sub>2</sub>O<sub>3</sub> coatings is very interesting. These results will be published elsewhere.

#### 4 Conclusions

Different phases of Al<sub>2</sub>O<sub>3</sub> like (i) pure α-Al<sub>2</sub>O<sub>3</sub> prepared by solution combustion method, (ii) pure γ-Al<sub>2</sub>O<sub>3</sub> prepared by

precipitation route and (iii) commercial Alcoa Al<sub>2</sub>O<sub>3</sub> containing mixture of α, γ and δ particles were codeposited with Ni at three different current densities and different magnetic stirring speeds. There was a change in the microstructure of the surface of the coatings based on the phases of the particle. A nodular nickel microstructure was observed with the incorporation of γ-Al<sub>2</sub>O<sub>3</sub> particles and the same was absent when pure α-alumina particles were incorporated. It was found that both the stirring speed and the applied current density have a profound effect on the particle incorporation and also to the extent of agglomeration. Ni-Al<sub>2</sub>O<sub>3</sub> containing pure α-phase exhibited the highest microhardness (550 HK). Irrespective of the current densities used for electrodeposition, lowest rpm results in larger agglomerated particles in case of Ni-Al<sub>2</sub>O<sub>3</sub>-1 and Ni-Al<sub>2</sub>O<sub>3</sub>-2. This phenomenon is not predominantly seen in Ni-Al<sub>2</sub>O<sub>3</sub>-3. Irrespective of the current densities always smaller particles were incorporated at the highest rotation speed (1000 rpm). The cross-sectional optical micrographs revealed the uniform distribution of particles in the Ni matrix with larger agglomerated particles in Ni-Al<sub>2</sub>O<sub>3</sub>-1 and Ni-Al<sub>2</sub>O<sub>3</sub>-2. In Ni-Al<sub>2</sub>O<sub>3</sub>-3, a uniform distribution of particles with very less agglomeration was observed. From this study it is evident that the source of particles, its properties (phase purity, particle shape, size, size distribution etc.), stirring speeds and current density are also the factors which govern the properties of the composite coating.

**Acknowledgements** The authors thank the Director, NAL-CSIR for giving permission to publish this work. The authors acknowledge Mr. N. Balaji for the help received in carrying out the experiments. The help received from Mrs. Latha for measuring the microhardness and recording the optical micrographs is greatly acknowledged. The support received from Mr. Siju (FESEM), Mr. Raghavendra (SEM), Dr. Anjana Jain (XRD), Dr. Ramachandra Rao (Particle size analysis) and Mr. Manikandanath (Raman spectra) is greatly acknowledged. FESEM work was supported by facility creation project of CSIR (FAC-00-01-11).

#### References

1. Bonino J-P, Loubiere S, Rousset A (1998) *J Appl Electrochem* 28:1227
2. Feng Q, Li T, Yue H, Qi K, Bai F, Jin J (2008) *Appl Surf Sci* 254:2262
3. Dong YS, Lin PH, Wang HX (2006) *Surf Coat Technol* 200:3633
4. Banovic SW, Barmak K, Marder AR (1999) *J Mater Sci* 34:3203
5. Du L, Xu B, Dong S, Yang H, Wu W (2005) *Surf Coat Technol* 192:311
6. Erler F, Jakob C, Romanus H, Spiess L, Wielage B, Lampke T, Steinhauser S (2003) *Electrochim Acta* 48:3063
7. Bund A, Thiemig D (2007) *Surf Coat Technol* 201:7092
8. Fawzy MH, Ashour MM, Abd El-Halim AM (1996) *Trans IMF* 74(2):72
9. Shao I, Verecken PM, Cammarate RC, Searson PC (2002) *J Electrochem Soc* 149:C610

10. Sautter FK (1963) J Electrochim Soc 110:557
11. Karayianni HS, Batis G, Vassiliou P (1999) Anti-Corros Methods Mater 46:29
12. Szczygiel B, Kolodziej M (2005) Electrochim Acta 50:4188
13. Thiemig D, Bund A, Talbot JB (2007) J Electrochim Soc 154:D510
14. Chen L, Wang L, Zeng Z, Xu T (2006) Surf Coat Technol 201:599
15. Wei X, Dong H, Lee C-H, Jiang K (2008) Mater Lett 62:1916
16. Ciubotariu A-C, Benea L, Magda L-V, Dragan V (2008) Electrochim Acta 53:4557
17. Hoffmann JE, Ernst RG (1964) Incra reports, Project. 31
18. Sautter FK (1963) J. Electrochim Soc 110:557
19. Chen ES, Lakshminarayanan GR, Sautter FK (1971) Met Trans 2(4):937
20. Patil KC, Aruna ST, Mimani T (2002) Curr Opin Solid State Mater Sci 6:507
21. Porto SPS, Krishnan RS (1967) J Chem Phys 47:1009
22. Aminzadeh A, Sarikhani-fard H (1999) Spectrochim Acta A 55:1421
23. Pavlatou EA, Spyrellis N (2008) Russ J Electrochim 44:745
24. Bercot P, Pena-Munoz E, Pagetti J (2002) Surf Coat Technol 157:282
25. Celis JP, Roos JR (1977) J Electrochim Soc 124:1508
26. Buelens C (1984) Thesis. Katholieke Universiteit te Leuven
27. Fransaer J, Celis JP, Roos JR, J Electrochim Soc 139:413
28. Low CTJ, Wills RJA, Walsh FC (2006) Surf Coat Technol 201:371